Supporting Information

Water-gel for gating graphene transistors

Beom Joon Kim,[†] Soong Ho Um,[†,‡] Woo Chul Song,[‡] Yong Ho Kim,[†,§] Moon Sung Kang,*[,#] and Jeong Ho Cho*[,†,‡]

[†]SKKU Advanced Institute of Nanotechnology (SAINT), [‡]School of Chemical Engineering, [§]Department of Chemistry, Sungkyunkwan University, Suwon, 440-746, Korea.
[#]Department of Chemical Engineering, Soongsil University, Seoul 156-743, Korea.

Correspondence and requests for materials should be addressed to M.S.K. (e-mail: mskang@ssu.ac.kr) or J.H.C. (e-mail: jhcho94@skku.edu).

Graphene growth. The graphene film was grown on a Cu foil by chemical vapour deposition in a quartz tube furnace. Typical growth processes were as follows. A Cu foil (25 μm, Alfa Aesar) was first inserted into a quartz tube which was inserted into a separate tube furnace. Such a double-walled structure was beneficial for minimizing the temperature gradient around the Cu foil. After degassing, the tube furnace was heated to 1000°C with a H_2 flow of 10 sccm. To reduce any copper (II) oxide on the surface of the foil, this temperature was maintained for 30 minutes. This led to the enlargement of the grain size of the Cu foil which was necessary to attain graphene films with larger grain sizes.[S1,2] Subsequently, a mixture of CH_4 (15 sccm) and H_2 (10 sccm) was delivered to the tube and the temperature was held at 1000°C for another 30 minutes. Finally, the CH_4 flow was disconnected and the furnace was cooled down to room

temperature quickly. During the cooling process, monolayer graphene was formed on both sides of the Cu foil.

Graphene transfer. The as-prepared graphene monolayer was transferred onto PET substrates through the following process. First, one side of the graphene/Cu foil was spin-coated with poly(methyl methacrylate) (PMMA) dispersed in chlorobenzene and cured at 70°C for 10 min. Subsequently, the other side of the foil was exposed to O_2 plasma for 2 s to remove the graphene monolayer grown on that side. Afterwards, the Cu foil was floated on an aqueous solution of 0.1 M ammonium persulphate ($(NH_4)_2S_2O_8$), which etched away the Cu foil present underneath. Once the Cu foil was fully removed, the remained PMMA/graphene film was scooped with a flat PET substrate. Finally, the PMMA layer on top of the graphene layer was removed by rinsing the scooped film with acetone and deionized water to yield a film of monolayer graphene on the PET substrate.

Cell viability test. Human prostate cancer cells (PC3) (1×10^5 cells per well) were seeded in 24-well plates and cultured to 70% confluence within complete growth media (RPMI 1640 supplemented with 10% fetal bovine serum). After 2 hours of incubation with highly concentrated Na-DNA (0.1 mM), the cells were washed with phosphate buffer solution (PBS) and further incubated in a fresh RPMI 1640 medium for 3, 6, 12, 24, 36 and 48 hours, respectively. After the incubation, 1 mL of RPMI 1640 medium containing 75 μM of propidium iodide (PI) was added into each well, followed by another incubation process under dark at 37 °C for 30 minutes. After washing with PBS, the cells were detached using trypsin-EDTA solution

and further washed with PBS three times. Finally, cell viability was assessed using a flow-cytometer (FACS-ARIA, BD Biosciences).

Impedance spectroscopy measurements. The capacitive behaviour of the *M*-DNA electrolytes was investigated through impedance spectroscopy measurements[S3] using coplanar MIM capacitor testbeds. The MIM testbeds were comprised of Au electrode/*M*-DNA electrolyte/Au electrode. The electrodes in a coplanar configuration were separated by 5 μm and the electrode areas varied between 1.00 and 0.05 mm^2. From the measured complex impedance ($Z=Z'+iZ''$) values as a function of frequency (f = 20~1,000,000 Hz), important parameters describing the electrical properties of the electrolyte could be determined. In particular, a simple equivalent circuit containing a resistor (with a resistance, R) connected in series to a capacitor (with a capacitance, C) was utilized.[S4] Here, the resistor reflects the finite ionic conductivity of the system, while the capacitor represents the electric double layers formed at the electrode/electrolyte interfaces. For an ideal resistor and capacitor connected in series, the Nyquist plot, a plot of $-Z''$ as a function of Z', should exhibit a straight vertical line. The experimental data from the Na-DNA electrolytes (8 μM), for example, did yield steep lines (**Figure S3a**) confirming the applicability of the series model. However, it should be noted that these lines exhibited finite slopes. Such non-ideal behaviour is often observed for electrolyte systems in contact with solid electrodes due to capacitance dispersion.[S5,6]

The plots of phase angle ($\tan\varphi = Z''/Z'$) *vs*. operation frequency (**Figure S3b**) reveal important insights. The phase angle was closer to -90° at low frequencies (an indication of a purely capacitive response of the system) but gradually became closer to 0° at higher frequencies

(an indication of a purely resistive response of the system). Therefore, the Na-DNA electrolytes behaved more like a capacitor at low frequencies but behaved more like a resistor at high frequencies. Interestingly, such transitional behaviour was delayed at higher frequencies for MIM test-beds with smaller electrode areas. The geometry-dependent results may be attributed to the unconventional device configuration of the coplanar capacitor configuration. Unlike typical capacitors with parallel electrodes in a sandwich structure, the electrical fields across the coplanar electrodes were not distributed uniformly. Namely, the electrical field lines between the near sides of the respective electrodes must be drawn denser than those connecting the far sides of the electrodes. As such, the variation in the electrical field would be amplified as the electrode area becomes larger (the far sides of the respective electrodes are separated further). Given that the separation between the electrodes are the same, the capacitive response for devices with smaller electrodes would be more efficient at high frequencies as compared to those with larger electrodes. Furthermore, the *C vs*. *f* plots (**Figure S3c**) can be drawn based on the -Z" versus *f* data (**Figure S3d**) using the relation C=-1/(2πfZ"). Consistent with the frequency-dependent φ data, the high capacity of the Na-DNA electrolytes was retained at higher frequencies when electrodes with smaller area were employed.

We also carried out similar sets of experiments using different types of *M*-DNA where the area of the coplanar gold contact was 0.05 mm^2. Na-, Mg-, Ca-, and Zn-DNA electrolytes yielded the expected steep line with finite slopes in the Nyquist plots (**Figure S4a**). Meanwhile, MIM samples with water (and the Fe-DNA electrolytes) showed a faint signature of a half circle on the left side of the steep line. As a half circle in the Nyquist plot reflects a system containing a resistor and a capacitor in parallel, the results may indicate the presence of an additional resistor component at the electrode/electrolyte interface in parallel to the original electric double layer

capacitor that was already connected in series with a resistor. This additional resistor component for water electrolytes can be attributed to the charge transfer reaction of water at the solid interface.

Figure S4b displays the φ versus f plots for different M-DNA electrolytes. Similar to the results from **Figure S3**, the dominant capacitive behaviour of the M-DNA electrolytes at low frequencies gradually transitioned to resistive behaviour at high frequencies. More importantly, such transitional behaviour took place at higher frequencies for Na-, Mg-, Ca-, Zn-, and Fe-DNA electrolytes in sequence. This implies that higher specific capacitance is achievable at higher frequencies when Na-DNA electrolytes are employed rather than other systems (**Figure S4c** and **d**). Also, from the frequency range exhibiting resistive behaviour (*i.e*. high frequency regime with $\varphi \sim 0$), the electrical resistance of the electrolyte could be extracted simply from Z'. Specifically, Z' should be equal to R if the electrolyte system behaves as a pure resistor, which is the case when $\varphi = 0$. These results together with the geometry of the device further lead to estimating the ionic conductivity of the M-DNA electrolytes that was used to draw **Figure 3b** in the main text.

Table S1. Summary of parameters extracted from impedance spectroscopy measurements.

	Resistance (kohm)	Ionic conductivity (mS)	Slope (Z" *vs*. f)	Capacitance (nF)
Water	11.39	0.09	-0.912	5.45
Na-DNA	0.86	1.17	-0.924	4.69
Mg-DNA	1.05	0.95	-0.918	5.52
Ca-DNA	1.24	0.81	-0.921	4.98
Zn-DNA	1.68	0.59	-0.923	4.42
Fe-DNA	3.71	0.26	-0.915	5.35

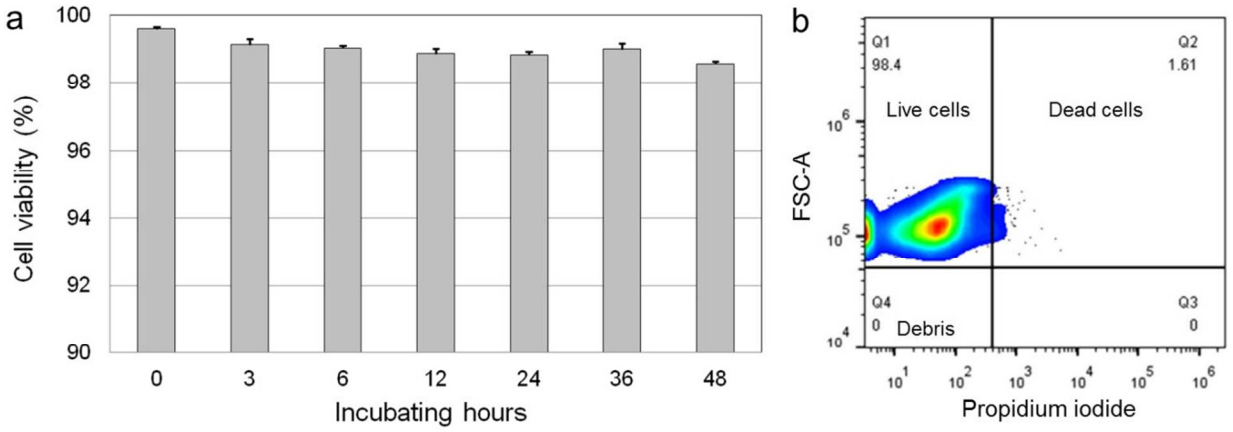

Figure S1. The cell viability test results for Na-DNA. (a) The viability of PC3 cell lines plotted as a function of incubating hours after exposure to highly concentrated Na-DNA (0.1 mM) for 2 hours. (b) Flow cytometric plot indicating most of cells are live after 48 hours.

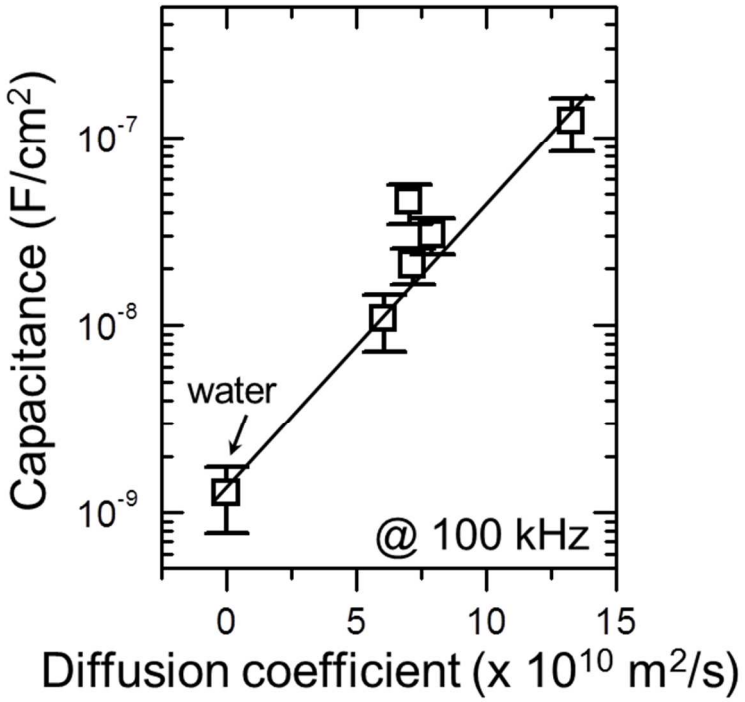

Figure S2. (Capacitance, Ionic conductivity)-Diffusion coefficient characteristic. Specific capacitance and ionic conductivity of *M*-DNA (*M* = Na, Mg, Ca, Fe, and Zn) water-gel as a function of diffusion coefficient.

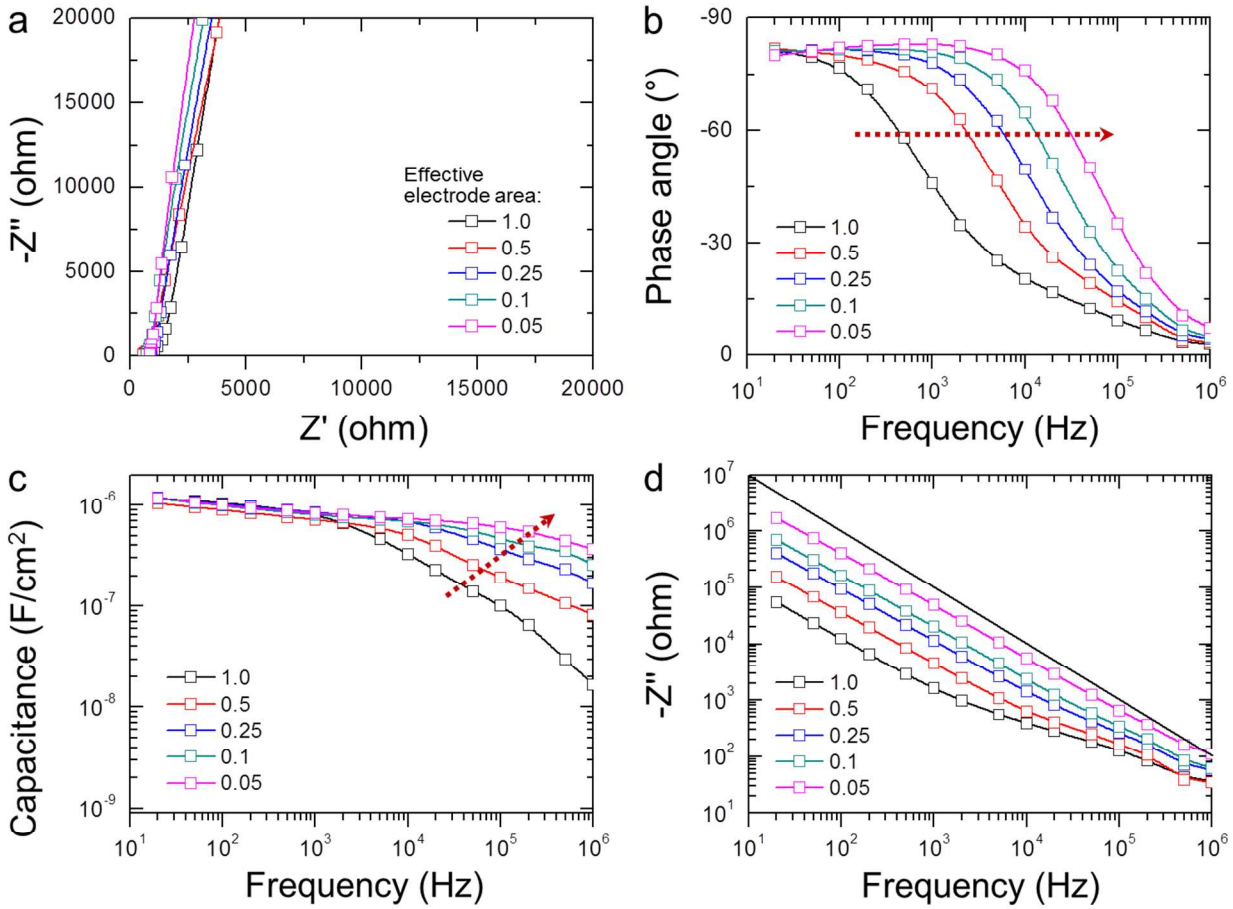

Figure S3. Impedance analysis (influence of effective electrode area in contact with electrolyte). (a) Nyquist plot for Na-DNA water-gel-based capacitors with different gold contact areas. (b) Plot of phase angle *vs*. frequency.(c) Plot of specific capacitance*vs*. frequency.(d) Plot of imaginary impedance *vs*. frequency.

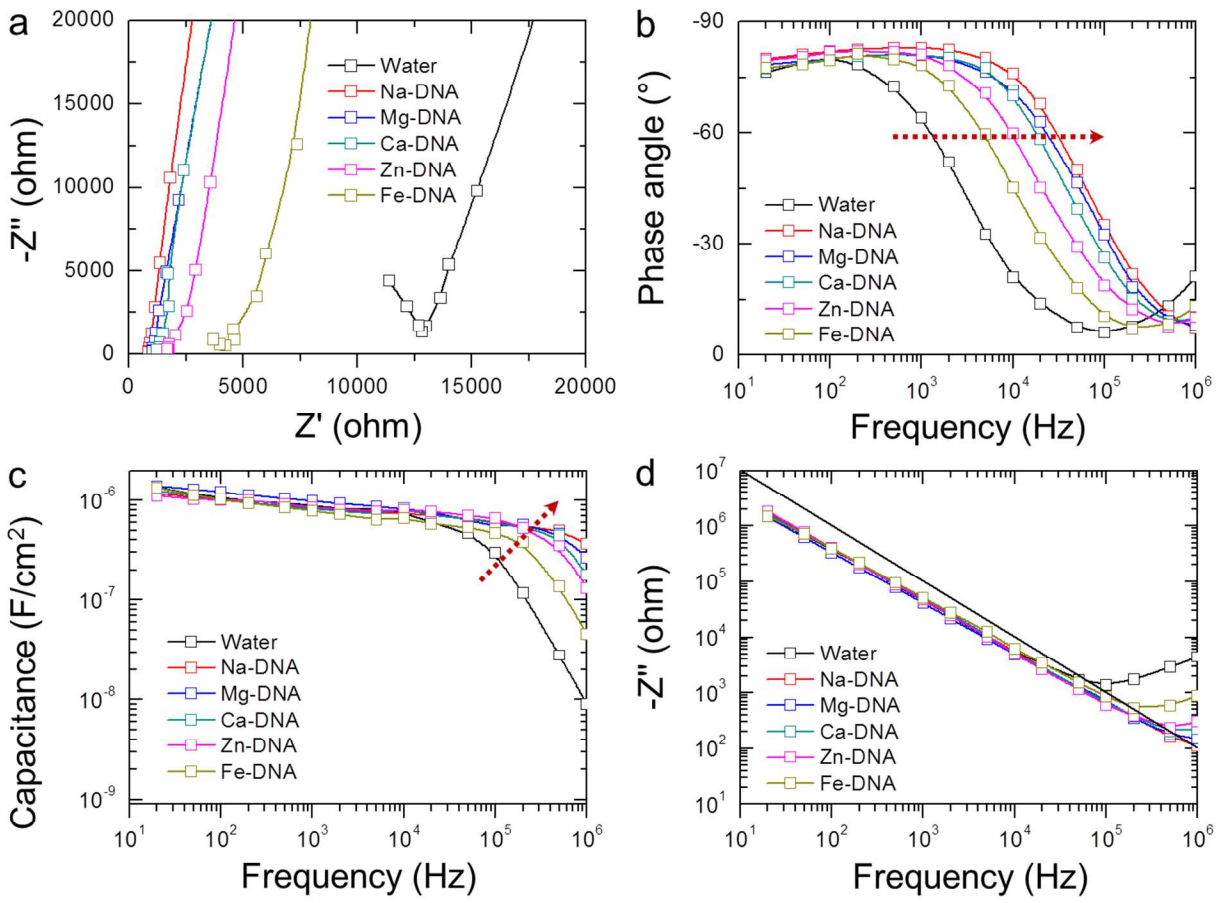

Figure S4. Impedance analysis (influence of metal cations of *M*-DNA electrolytes). (a) Nyquist plot for water and *M*-DNA water-gel-based capacitors with different metal cations. (b) Plot of phase angle *vs*. frequency. (c) Plot of specific capacitance *vs*. frequency. (d) Plot of imaginary impedance *vs*. frequency. The effective area of the electrode is 0.05 mm^2.

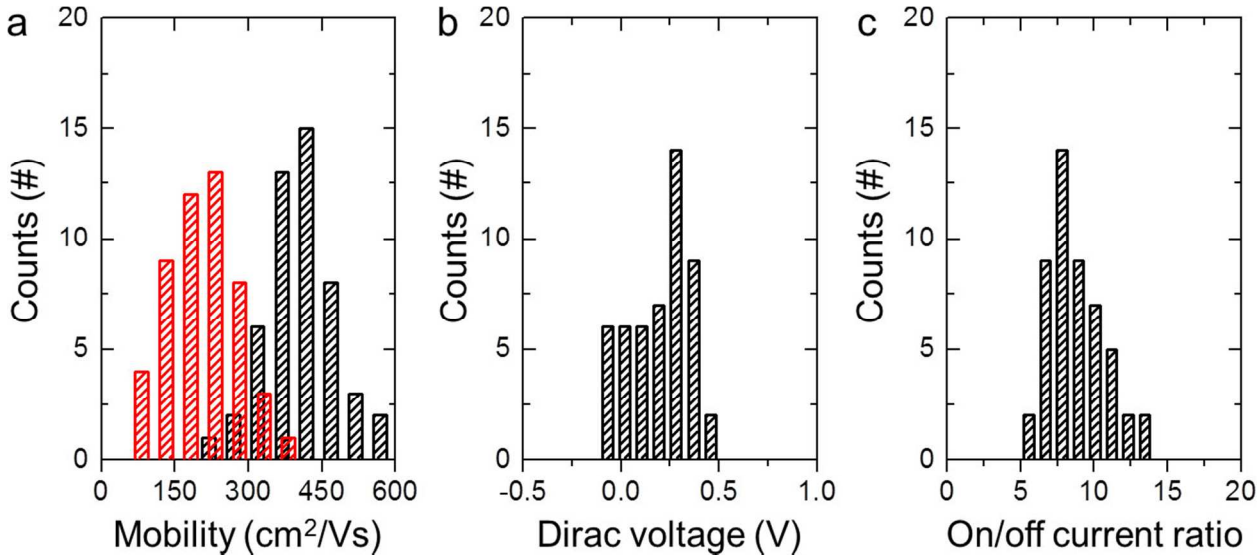

Figure S5. Histograms of (a) the hole (black)/electron (red) mobilities, (b) the Dirac voltage, and (c) the on/off current ratio for the Na-DNA water-gel-gated graphene transistors (total 50 devices).

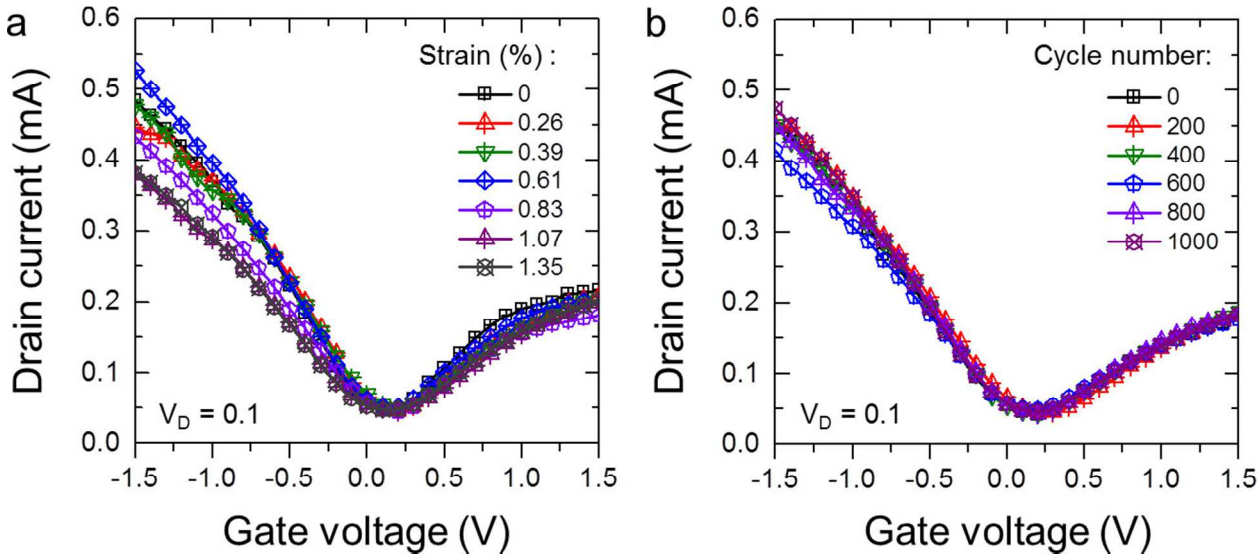

Figure S6. (a) Transfer characteristics measured at different strain levels (0-1.35%) and (b) those after different cycles of bending/releasing (0-1000) for a Na-DNA water-gel-gated graphene FET on a PET substrate.

Reference

S1 Li, X., Cai, W., An, J., Kim, S., Nah, J., Yang, D., Piner, R., Velamakanni, A., Jung, I. & Tutuc, E. Large-area synthesis of high-quality and uniform graphene films on copper foils. *Science* **324**, 1312-1314 (2009).

S2 Mattevi, C., Kim, H. & Chhowalla, M. A review of chemical vapour deposition of graphene on copper. *J. Mater. Chem.* **21**, 3324-3334 (2011).

S3 Brug, G., Van Den Eeden, A., Sluyters-Rehbach, M. & Sluyters, J. The analysis of electrode impedances complicated by the presence of a constant phase element. *Journal of electroanalytical chemistry and interfacial electrochemistry* **176**, 275-295 (1984).

S4 Lee, K. H., Zhang, S., Lodge, T. P. & Frisbie, C. D. Electrical Impedance of Spin-Coatable Ion Gel Films. *J. Phys. Chem. B* **115**, 3315-3321 (2011).

S5 Pajkossy, T. Impedance of rough capacitive electrodes. *Journal of Electroanalytical Chemistry* **364**, 111-125 (1994).

S6 Pajkossy, T. Impedance spectroscopy at interfaces of metals and aqueous solutions—Surface roughness, CPE and related issues. *Solid State Ionics* **176**, 1997-2003 (2005).